OPTICS

All-optical reversible single-photon isolation at room temperature

Ming-Xin Dong[1,2], Ke-Yu Xia[3,4]*, Wei-Hang Zhang[1,2], Yi-Chen Yu[1,2], Ying-Hao Ye[1,2], En-Ze Li[1,2], Lei Zeng[1,2], Dong-Sheng Ding[1,2]*, Bao-Sen Shi[1,2]*, Guang-Can Guo[1,2], Franco Nori[5,6]

Nonreciprocal devices operating at the single-photon level are fundamental elements for quantum technologies. Because magneto-optical nonreciprocal devices are incompatible for magnetic-sensitive or on-chip quantum information processing, all-optical nonreciprocal isolation is highly desired, but its realization at the quantum level is yet to be accomplished at room temperature. Here, we propose and experimentally demonstrate two regimes, using electromagnetically induced transparency (EIT) or a Raman transition, for all-optical isolation with warm atoms. We achieve an isolation of 22.52 ± 0.10 dB and an insertion loss of about 1.95 dB for a genuine single photon, with bandwidth up to hundreds of megahertz. The Raman regime realized in the same experimental setup enables us to achieve high isolation and low insertion loss for coherent optical fields with reversed isolation direction. These realizations of single-photon isolation and coherent light isolation at room temperature are promising for simpler reconfiguration of high-speed classical and quantum information processing.

INTRODUCTION

In analogy to counterparts widely used in electronic circuits, optical nonreciprocal devices, such as isolators and circulators, play a fundamental role in modern optical communications and now are even crucial for quantum information processing (*1*). Single photons are ideal for encoding and transporting quantum information, thanks to the no-cloning theorem of quantum mechanics (*2*). In this regard, a nonreciprocal photonic device operating at the single-photon level is highly desirable as a building block for quantum information processing, quantum networks (*1*, *3*, *4*), quantum transistors (*5*), quantum routers (*6*), and quantum computation (*7*).

To achieve optical nonreciprocity (ONR), one needs to break Lorentz reciprocity (*8*–*10*). Conventionally, ONR can be achieved with bulky magneto-optical materials and a strong external magnetic field, thus incompatible with on-chip systems and magnetic-sensitive quantum information processing. The alternative approach based on nonlinearity has been attempted for decades (*10*). However, these nonlinear nonreciprocal devices are not suitable for a weak field because of dynamic reciprocity (*11*). Other all-optical approaches using optomechanics (*12*–*15*), phonon-induced Brillouin scattering (*16*), and parity-time symmetry broken systems (*17*–*20*) have been reported. Despite its success for classical fields, the thermal phononic excitation in optomechanical systems (*21*, *22*) or material gain in parity-time symmetry breaking cause strong noise and destroy the quantum nature of single photons. Recently, atomic systems (*23*–*30*) and chiral quantum optical systems (*1*, *31*, *32*) have also been exploited to achieve photon isolation. Although many efforts have been devoted to photonic isolation at the quantum level (*1*, *23*–*29*, *32*–*34*), the experimental realization of all-optical isolation for both genuine single photons and classic fields is still extremely challenging, in particular, at room temperature.

Electromagnetically induced transparency (EIT) (*35*, *36*) has been a powerful tool for manipulating quantum fields, such as the memory of nonclassical fields (*37*, *38*). Here, we report an experimental realization of a single-photon ONR and coherent light isolation by using atomic EIT and Raman regimes, respectively, at room temperature without applying a magnetic field. The input single photons maintain their quantum nature with high transmission in the chosen transparent direction. In contrast, the unwanted back reflection is mostly completely blocked. In addition, we observe a direction-reversible ONR for the EIT and Raman regimes. The demonstration of all-optical ONR for single photons, as well as the reversible ONR transmission, paves the way toward reconfigurable nonreciprocal information processing.

Experimental setup

As schematically depicted in Fig. 1A, we create a nonreciprocal optical system using a thermal atomic ensemble in a ladder-type configuration in which the signal field Ω_p couples to the atomic transition of $|1\rangle \rightarrow |2\rangle$ with a detuning $\Delta\omega_p$, and the control field Ω_c drives the transition $|2\rangle \rightarrow |3\rangle$ with a detuning $\Delta\omega_c$ (not shown in Fig. 1A). Here, Ω_p and Ω_c denote the Rabi frequencies of the signal and control fields, respectively. The relevant quantum states $|1\rangle$, $|2\rangle$, and $|3\rangle$ correspond to the ^{85}Rb atomic levels $5S_{1/2}(F = 3)$, $5P_{3/2}(F' = 3)$, and $5D_{5/2}(F'' = 4)$, respectively. Because of the microscopic Doppler effect of atoms, the signal and control fields are both subject to a direction-dependent Doppler frequency shift seen by the warm atoms. We denote the forward (backward) propagation as the transmission of photons from port 1 (2) to port 2 (1); meanwhile, the photons counter-propagate (co-propagate) with a right-to-left propagating control field, as shown in Fig. 1B. In the forward case, an atom always "sees" the signal and control fields with

[1]Key Laboratory of Quantum Information, University of Science and Technology of China, Hefei, Anhui 230026, China. [2]Synergetic Innovation Center of Quantum Information and Quantum Physics, University of Science and Technology of China, Hefei, Anhui 230026, China. [3]National Laboratory of Solid State Microstructures, Collaborative Innovation Center of Advanced Microstructures, College of Engineering and Applied Sciences, and School of Physics, Nanjing University, Nanjing 210093, China. [4]Key Laboratory of Intelligent Optical Sensing and Manipulation (Nanjing University), Ministry of Education, Nanjing 210093, China. [5]Theoretical Quantum Physics Laboratory, RIKEN Cluster for Pioneering Research, Wako-shi, Saitama 351-0198, Japan. [6]Physics Department, The University of Michigan, Ann Arbor, MI 48109-1040, USA.
*Corresponding author. Email: keyu.xia@nju.edu.cn (K.-Y.X.); dds@ustc.edu.cn (D.-S.D.); drshi@ustc.edu.cn (B.-S.S.)

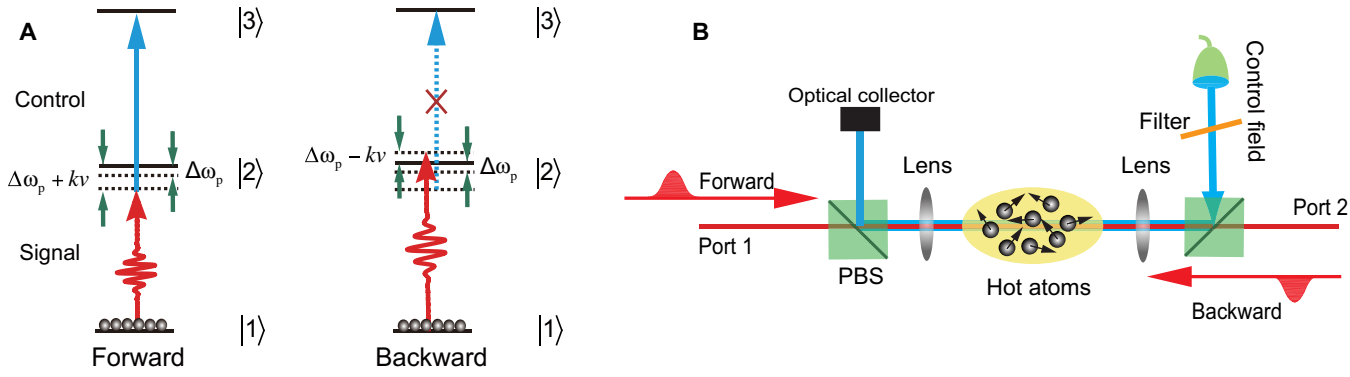

Fig. 1. Schematic energy-level diagram and experimental setup for room temperature all-optical isolation. (**A**) Level diagrams of the ladder-type atomic configurations for the EIT regime in the forward and backward cases, corresponding to Doppler-free and Doppler-broadened cases, respectively. The two-photon resonance condition holds in the forward case, whereas the two-photon transition is far off-resonance in the backward case. The wavelengths of the signal and control field are 780 and 776 nm, respectively. (**B**) Experimental setup. PBS, polarization beam splitter. The signals are sent to the nonreciprocal device along two opposite directions to demonstrate the single-photon and classical ONR, for the EIT and Raman regimes, respectively.

opposite Doppler frequency shifts. For example, a left-moving atom at velocity v may couple to the forward-propagating signal field with a Doppler shift of $+k_p v$, but to the control field with shift $-k_c v$, where k_p (k_c) is the wave vector amplitude of the signal (control) field, $k_p \approx k_c$, and v is the randomly distributed velocity of atoms. In our experiment using room temperature Rb atoms, the difference $|(k_p - k_c)v|$ is a few megahertz much smaller than the Doppler broadening. We neglect its effect on the two-photon detuning. For simplicity, we take $k_p = k_c = k$.

Generally, EIT can be interpreted as a result of the cancellation of single-photon absorption by quantum destructive interference of two transition pathways between the level $|1\rangle$ and two dressed states consisting of levels $|2\rangle$ and $|3\rangle$, which are driven by a strong resonant control field. In the EIT regime, we take $|\Omega_c| \gg |\Omega_p|$, and $\Delta\omega_c = -\Delta\omega_p$, as shown in Fig. 1A. The Doppler shifts of the near-resonant signal and control fields have opposite signs in the forward-propagation case. Their impact on two-photon detuning $\Delta = \Delta\omega_p + \Delta\omega_c$ is cancelled. Thus, the overall two-photon detuning is negligible in this ladder-type configuration, and our system is almost Doppler-free for the forward signal. In this case, quantum interference between two transition pathways is destructive, disabling the single-photon absorption. The absorptive atoms become nearly transparent to the resonant signal and EIT occurs (*39*). In contrast, in the backward case, the signal and control fields undergo the same Doppler shift because they propagate in the same direction. Thus, the two-photon transition is detuned by $2kv$, far away from the two-photon resonance. The quantum interference is too weak. Therefore, hot atoms block the propagation of the backward-moving signal.

The Raman regime (see Fig. 4A) provides a different mechanism for achieving ONR. In the Raman regime, the single-photon detunings, $\Delta\omega_c$ and $\Delta\omega_p$, are larger than the atomic Doppler broadening. Thus, the single-photon absorption of the signal is negligible, but the two-photon absorption becomes dominant via Raman transitions. In contrast to the EIT regime, when the Doppler shifts of the signal and control fields cancel each other, the signal field is subject to two-photon resonance absorption in the Raman regime. In the backward case, the Doppler effect breaks the two-photon resonance condition. As a result, the signal can pass through atoms with little absorption. Using such chiral two-photon resonance configuration, we can reverse the ONR with respect to the EIT regime. Note that an alternating-current (AC) Stark shift δ resulting from the strong control field needs to be taken into account in the Raman regime. In the experiments, we adjust the control field frequency to $\Delta\omega_c = -\Delta\omega_p + \delta$, to compensate for the AC Stark shift such that the effective two-photon detuning is vanishing small. Without the offset δ from $-\Delta\omega_p$, the two-photon resonance condition may break when the control field is too strong.

Theoretical model

The chiral response of hot atoms to the signal field under the auxiliary control laser light can be used to break Lorentz reciprocity. To further characterize this ONR, we derive the susceptibilities, χ_{fw} and χ_{bw}, for the forward and backward propagation cases by solving the steady-state solution of the master equation, obtaining

$$\chi_{fw} = \int_{-\infty}^{+\infty} \frac{iN(v)\mu_{21}^2/(\hbar\varepsilon_0)}{\gamma_{21} - i(\Delta\omega_p + kv) + \frac{\Omega_c^2/4}{\gamma_{31} - i\Delta}} dv \quad (1)$$

$$\chi_{bw} = \int_{-\infty}^{+\infty} \frac{iN(v)\mu_{21}^2/(\hbar\varepsilon_0)}{\gamma_{21} - i(\Delta\omega_p - kv) + \frac{\Omega_c^2/4}{\gamma_{31} - i(\Delta - 2kv)}} dv \quad (2)$$

where $\Delta = \Delta\omega_p + \Delta\omega_c$ is the two-photon detuning, $N(v) = N_0 e^{-v^2/u^2}/(u\sqrt{\pi})$ denotes the velocity distribution of atoms, u is the most probable velocity, and N_0 is the density of atoms. In addition, μ_{21} is the corresponding dipole moment of the $|1\rangle \rightarrow |2\rangle$ transition, and γ_{21} (γ_{31}) is the dephasing rate between levels $|2\rangle$ and $|1\rangle$ ($|3\rangle$ and $|1\rangle$).

Here, we consider that the signal field only causes a weak perturbation to the atoms in comparison with the strong control field that forces atoms to be primarily populated in the state $|1\rangle$. This prerequisite is reasonable when the control field is much stronger than the signal field, i.e., $|\Omega_c| \gg |\Omega_p|$. Clearly, the susceptibility of atoms is chiral for oppositely propagating signal fields, leading to completely different transmissions, T_{fw} and T_{bw}, in the forward and backward propagation cases (see Materials and Methods).

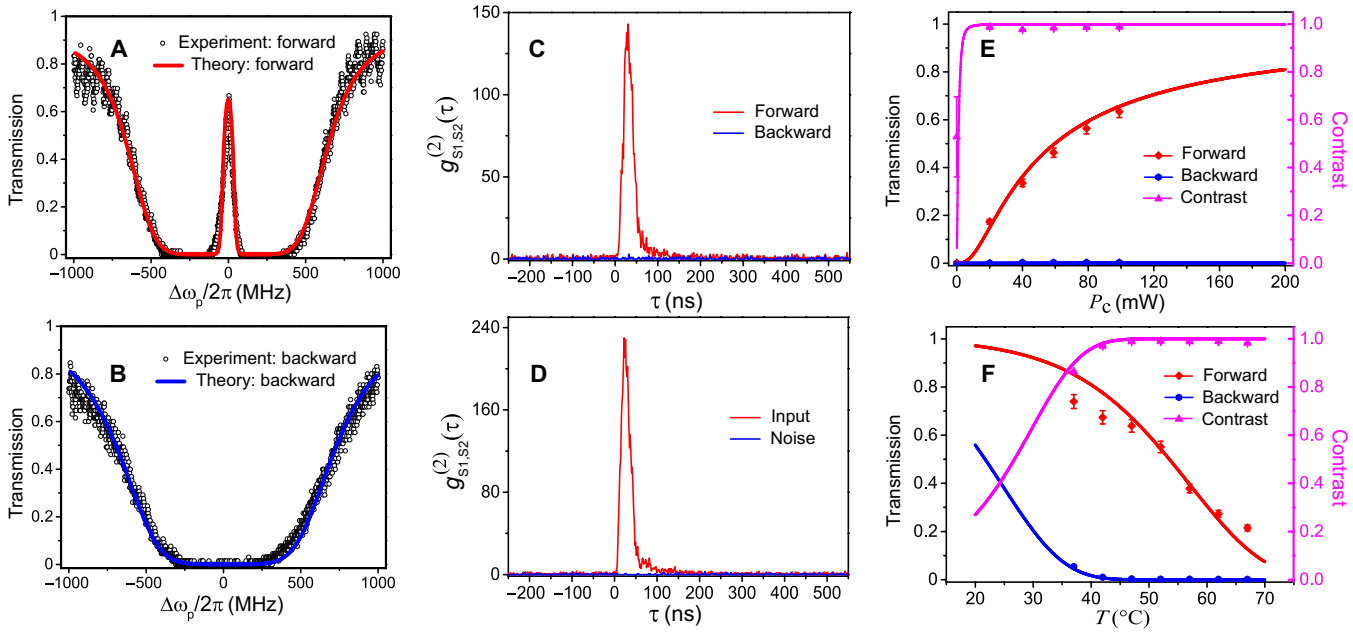

Fig. 2. Single-photon ONR working in the EIT regime. (**A** and **B**) The measured forward (backward) transmission spectra of the signal as a function of the signal detuning from the atomic resonance $|1\rangle \rightarrow |2\rangle$. The red (blue) line is the theoretical fit by using Eq. 5, with $\gamma_{31} = 2\pi \times 5.5$ MHz, $\gamma_{21} = 2\pi \times 60$ MHz, $\Omega_c = 2\pi \times 320$ MHz, and the atomic ensemble length $L_{eff} = 2.8$ cm. (**C**) The measured second-order cross-correlated functions $g^{(2)}_{S1,S2}(\tau)$ of heralded single photons after propagating through the atomic vapor in the forward (red curve) and backward (blue curve) directions. (**D**) The second-order cross-correlated function of the input single photons (red curve) before the atomic vapor and the noise (blue curve). (**E**) and (**F**) show the forward transmission, backward transmission, and isolation contrast versus the power of the control field ($T = 48$°C) and the temperature of atomic vapor ($P_c = 100$ mW), respectively, when $\Delta\omega_p = 0$. The solid curves are the theoretical fits using Eq. 5. The error bars are estimated from Poisson statistics and represent a ±1 SD.

RESULTS

Single-photon ONR based on the EIT regime

The ONR for genuine single photons is implemented by using the experimental setup shown in Fig. 1B. First, we prepare a single S2 photon heralded by the detection of the S1 photon (see Materials and Methods for more details) through a spontaneous four-wave mixing (SFWM) (*40*, *41*) process in a cold atomic ensemble. The signal photons and the control field are both focused by a lens with a focal length of 300 mm onto the vapor cell. The beam waist for both the signal and control fields is $\omega_0 \sim 100$ μm. To obtain enough power for the control field, we place a tapered amplifier (TA) after a 776-nm diode laser. A tilted 780-nm bandpass filter (Semrock LL01-780-12.5), depicted in Fig. 1B, is subsequently used to work as a 776-nm filter to reduce the residual 780-nm laser in the control field induced by the amplified spontaneous emission of the TA. Furthermore, before the signal going to the detector, two 780-nm bandpass filters and two homemade Fabry-Perot etalons (50% transmittance and 500 MHz bandwidth) are inserted for further frequency filtering. Thanks to the distinguishable wavelength difference, 780 − 776 = 4 nm, between the signal and control field, the signal can be easily filtered out from the noise caused by the control field.

To evaluate the performance of ONR based on EIT, we first measure the transmission spectra in the forward and backward cases by scanning the detuning of the signal from $-2\pi \times 1000$ to $+2\pi \times 1000$ MHz, as depicted in Fig. 2 (A and B). To do this, we use a weak coherent light as input. The temperature of the atomic vapor is set to be 48° C, for example. Because the focused control field is nonuniform in the vapor cell, it is hard to match the spatial mode of the signal and control field perfectly in experiments (*42*). Thus, for simplicity, we estimate the Rabi frequency of the control field at the central of the vapor cell. We observe a high transmission contrast as long as the signal is resonant with the transition $|1\rangle \rightarrow |2\rangle$ and obtain ONR with a bandwidth of about $2\pi \times 200$ MHz (see Fig. 2, A and B).

To test the quantum character of nonclassical fields working under the EIT condition (*37*, *38*) in the ONR process, we input the heralded single photons with zero detuning, i.e., $\Delta\omega_p = 0$, and measure the normalized second-order cross-correlated function $g^{(2)}_{S1,S2}(\tau)$ in the forward and backward propagation cases. This function is defined as $g^{(2)}_{S1,S2}(\tau) = \langle \hat{a}^{\dagger}_{S1}(t)\hat{a}^{\dagger}_{S2}(t+\tau)\hat{a}_{S2}(t+\tau)\hat{a}_{S1}(t)\rangle / \left[\langle \hat{a}^{\dagger}_{S1}(t)\hat{a}_{S1}(t)\rangle\langle \hat{a}^{\dagger}_{S2}(t+\tau)\hat{a}_{S2}(t+\tau)\rangle\right]$, where $\hat{a}^{\dagger}_{S1}(t)$ $\left(\hat{a}^{\dagger}_{S2}(t+\tau)\right)$ and $\hat{a}_{S1}(t)$ $\left(\hat{a}_{S2}(t+\tau)\right)$ denote the photon creation and annihilation operators for the S1 (S2) photon at time t $(t+\tau)$, respectively. This formula describes the conditional probability when the S1 photon is detected at moment t, and the S2 photon will be detected at $t+\tau$, revealing the time correlation of the photon sources (*43*). The measured $g^{(2)}_{S1,S2}(\tau)$ of the transmitted photons in the forward (red line) and backward (blue line) cases are shown in Fig. 2C, where the obtained maximum bandwidth of the single photon pulses directly generated from the cold atoms is ~40 MHz. We evaluate the forward transmission as $T_{fw} = CC_{fw}/CC_{in}$ and the isolation as $I_{bw} = -10 \log (CC_{bw}/CC_{fw})$. Here, CC_{in} and CC_{fw} (CC_{bw}) represent the total integral coincidence counts for the initial input signal field and that after forward (backward) propagation, respectively. We obtain $T_{fw} = 63.8 \pm 1.5\%$ and $I_{bw} = 22.52 \pm 0.10$ dB. The isolation contrast, given by $\eta = (CC_{fw} - CC_{bw})/(CC_{fw} + CC_{bw})$ between these two cases, is $98.88 \pm 0.03\%$, revealing a strong single-photon ONR in this regime.

Figure 2D shows the second-order cross-correlated functions of the input signal photon (red line) and the noise (blue line). The

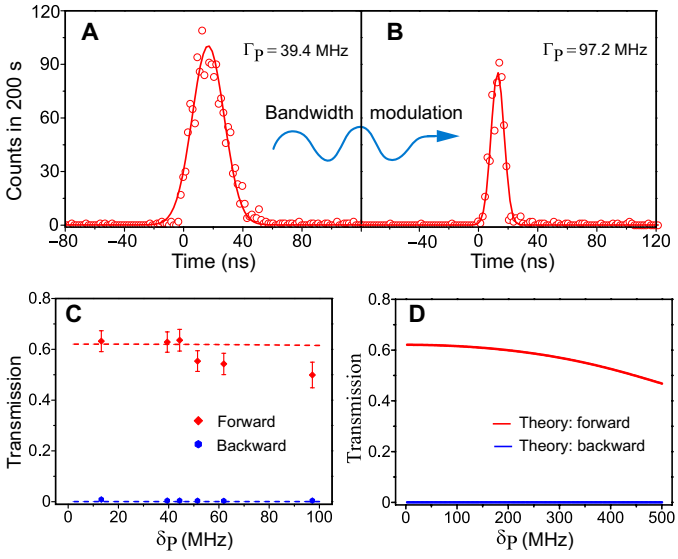

Fig. 3. Single-photon ONR. (**A**) The measured temporal wave packets of single-photon pulses generated from a cold atomic ensemble. The maximum bandwidth of single photons obtained from cold atoms without any modulation is ~40 MHz. (**B**) The modulated temporal wave packets of the single-photon pulse through a fiber EOM. The blue curve between (A) and (B) denotes the variation of single-photon bandwidth. (**C**) The forward and backward transmissions as a function of the single-photon bandwidth δ_p. The error bars in the experimental data are estimated from Poisson statistics and represent ± 1 SD. The dashed lines are the theoretical fits. (**D**) The theoretical ONR versus the bandwidth of the input single photons.

accidental coincidence from noise is measured to be 0.1%, by blocking the signal while keeping the applied control field. To evaluate the effect of noise on the quantum nature of single photons, we further measure a heralded autocorrelation parameter α by conducting a Hanbury-Brown-Twiss experiment. The parameter α can be used to benchmark the single-photon property, as defined in Materials and Methods. We obtain $\alpha = 0.031 \pm 0.002$ for the input-heralded single photons and $\alpha = 0.071 \pm 0.006$ for photons passing through the nonreciprocal system in the forward direction. This means that the single-photon property is preserved in this case. Here, the increase in α is mainly caused by the attenuation of single photons. In addition, we calculate the Cauchy-Schwarz inequality (*44*–*46*) factor *R* (see Materials and Methods) to study the variation of the nonclassical correlation between the signal and trigger photons in the nonreciprocal process. The nonclassical correlation of two photons is $R = 5.11 \times 10^3$ in the forward case, clearly violating the Cauchy-Schwarz inequality. In stark contrast, we have $R = 0.56$ in the backward case, indicating the breaking of the nonclassical correlation. Hence, the quantum nature of single photons is maintained in the forward case, while it is completely obliterated when entering the atomic vapor in the opposite direction.

The forward and backward transmissions versus the power of the control field are shown in Fig. 2E. The forward transmission increases first quickly and then approaches saturation as the control field power P_c increases. As expected, the backward transmission remains negligibly small. Limited by the experimentally available control field power up to $P_c = 100$ mW, the maximal forward transmission is measured to be ~63.8%, corresponding to an insertion loss of $-10 \log (T_{fw}) = 1.95$ dB. Theoretically, the forward transmission can be improved by applying a stronger control field. For example, the transmission T_{fw} can reach 80% when $P_c = 200$ mW, reducing the insertion loss to ~1 dB.

Figure 2F shows the transmission as a function of the temperature of the atomic vapor when $P_c = 100$ mW. Both of the forward and backward transmissions decrease with increasing temperature. This temperature dependence is also well fit theoretically. It can be seen that the forward transmission and the isolation contrast are high over the temperature range between 40°C and 50°C.

Furthermore, we investigate the ONR bandwidth for a single-photon input. We modulate the coherent time of heralded single photons, i.e., photon's bandwidth through a fiber electro-optic modulator (EOM) controlled by the arbitrary function generators (Tektronix, AFG3252) triggered by the detection of the S1 photon (*47*). By changing the duty cycle of the transistor-transistor-logic signals from the function generators, the single-photon bandwidth is changed, as shown in Fig. 3 (A and B). In our experiment, the single-photon bandwidth δ_p can be tuned between 13.2 and 97.2 MHz. The available maximum single-photon bandwidth is mainly limited by the rising time of the electric pulse produced by the function generator. Under this circumstance, we investigate the single-photon ONR with different bandwidth (see Fig. 3C). We observe a high isolation contrast even when the single-photon bandwidth is about 100 MHz. The theoretical calculation (dashed curves) is in good agreement with experimental observations.

As shown in the pink EIT region of Fig. 3D, the theoretical results indicate a 500-MHz bandwidth single-photon transmission ONR window. Both our experimental observations and theoretical model demonstrate a strong ONR for single photons with a bandwidth of hundreds of megahertz, allowing high-speed nonreciprocal quantum information processing.

Reversed ONR in the Raman regime

In recent decades, the Doppler-free two-photon transition process (*48*) has attracted considerable interest for many applications in atomic spectroscopy. Here, we exploit chiral two-photon absorption processes, i.e., Raman transitions (*49*, *50*), together with the Doppler effect to achieve ONR. The Raman regime shown in Fig. 4A can realize ONR as follows. The signal is detuned from the corresponding single-photon transition by $\Delta\omega_p = 2\pi \times 956$ MHz, larger than the atomic Doppler broadening $\Gamma/2 = 2\pi \times 600$ MHz. Without a control field, the one-photon absorption of the signal is negligible. Thus, the atomic vapor is nearly transparent to the signal in both the forward and backward cases.

Then, we consider a right-to-left moving control field driving the transition between levels $|2\rangle$ and $|3\rangle$. Because of the Doppler effect, this unidirectional control field allows a chiral two-photon absorption of the signal field, causing a nonreciprocal signal transmission. Note that the control field with Rabi frequency Ω_c and detuning $\Delta\omega_c$ induces an AC Stark shift δ to levels $|2\rangle$ and $|3\rangle$ (*51*). Without considering this shift, the two-photon resonance requires $\Delta\omega_c = -\Delta\omega_p$.

Now, we consider the AC Stark effect. To a good approximation, this AC Stark shift can be estimated as $\delta = \Omega_c^2/4\Delta\omega_p$, about few tens of megahertz (*51*). This shift adds an additional detuning δ to the two-photon resonance condition. Thus, it can reduce the two-photon absorption in the forward case and subsequently decrease the isolation contrast. To eliminate the detrimental effect of the AC Stark shift on the performance of the ONR, we slightly adjust the control field frequency such that $\Delta\omega_c = -\Delta\omega_p + \delta$ in both the forward

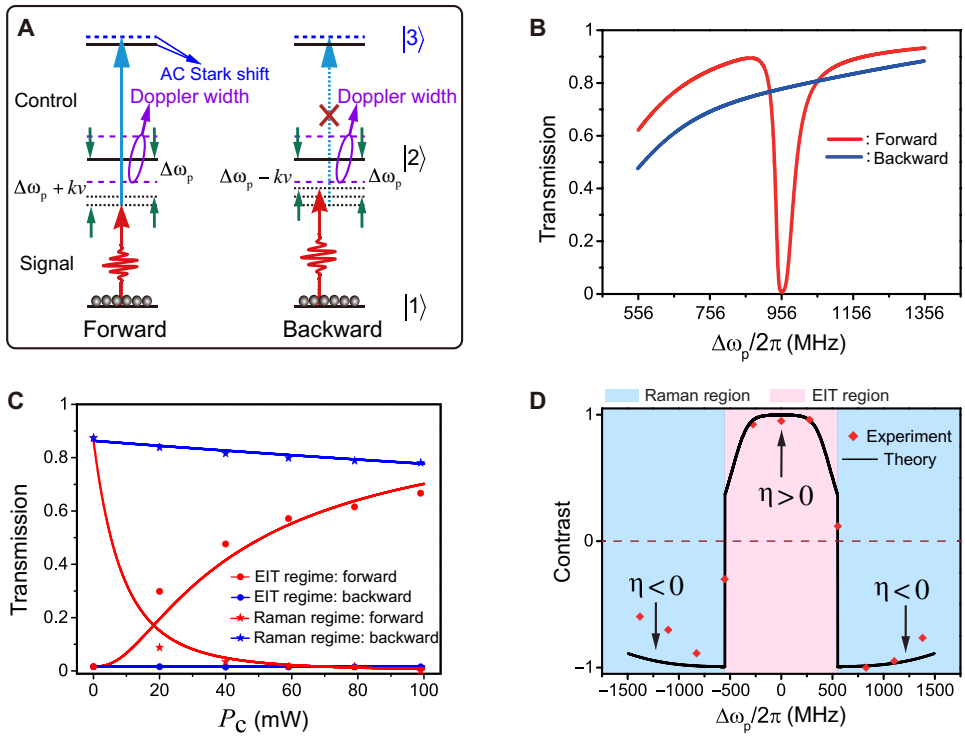

Fig. 4. Reversing ONR in the Raman regime. (**A**) Schematic of the energy level configuration with signals far detuned away from the resonant transition in the forward and backward cases, respectively. (**B**) The theoretical forward and backward transmissions. (**C**) Reversed transmissions in the EIT and Raman regimes as a function of the control field power. Experimental data are theoretically fit (solid curves) by using Eq. 5. (**D**) Isolation contrast versus the single-photon detuning of the signal.

and backward cases (see Fig. 4A). In doing so, we improve the isolation contrast as desired. We also apply $|\Omega_c| \gg |\Omega_p|$ so that the level $|1\rangle$ is primarily populated. Then, we consider that the signal induces a weak perturbation to atoms and derive the analytic forms of the susceptibilities given in Eqs. 1 and 2 using perturbation theory. Our theoretical model predicts nonreciprocal transmission of the signal (see Fig. 4B). Its validity is proved by the good agreement between the theoretical results and the experimental data shown in Fig. 4C.

In the forward case, the control field propagates along the opposite direction of the signal. We offset the control field frequency such that $\Delta\omega_c = -\Delta\omega_p + \delta$ to satisfy the effective two-photon resonance between states $|1\rangle$ and $|3\rangle$. In this case, the Doppler shifts of the control and signal fields cancel each other. The control field Ω_c strongly modifies the atomic susceptibility χ_{fw} in Eq. 1 and subsequently causes a two-photon near-resonance absorption of the signal field (see the red curve in Fig. 4B). In contrast, the control field co-propagates with the signal field in the backward case. The Doppler effect results in a large two-photon detuning $2kv$ in χ_{fw} (see Eq. 2). This large detuning greatly suppresses the modulation of the control field in the susceptibility χ_{fw} and prevents the signal from the two-photon absorption. Hence, the signal can pass through the atomic vapor with high transmission (see the blue curve in Fig. 4B).

The theoretical transmission spectra as a function of single-photon detuning in these two cases are shown in Fig. 4B. According to Eq. 5, the signal in the backward case can transmit through atoms with a fractional loss because both the single-photon and two-photon transitions are far-detuned from the atomic transition. Different from the backward case, a transmission dip appears around $\Delta\omega_p = 2\pi \times 956$ MHz in the forward case due to the Raman absorption caused by the resonant two-photon transition. Therefore, a strong ONR is obtained in the vicinity of $\Delta\omega_p = 2\pi \times 956$ MHz, but with a reversed ONR direction compared to the EIT regime.

In the following, we compare the nonreciprocal behavior of the Raman and EIT regimes by using a weak coherent light as input. As shown in Fig. 4C, the ONR in the Raman regime is reversed in comparison with the EIT regime. For example, when $P_c = 100$ mW, the signal in the EIT regime can transmit from port 1 to port 2 and is blocked in the opposite direction. On the contrary, the transmission from port 2 to port 1 is large and the opposite transmission is low in the Raman regime. Note that ONR based on the EIT and Raman regimes are induced by the thermal motion of atoms. In both regimes, the forward-moving signal and unidirectional control field satisfy the two-photon resonance condition. However, the unidirectional control field induces a different optical response of the atoms to the forward-moving signal, leading to the opposite ONR. Hence, the underlying physical mechanisms in these two regimes are different. In the EIT regime, the transparency window results from the destructive interference effect. In contrast, in the Raman regime, a virtual level is created by the pump of control field without interference effect, resulting in the two-photon-transition absorption of the signal.

The study of subtle differences between two similar quantum optics processes is of great interest in fundamental physics (*52*). Our experiment clarifies how the transition between the EIT and Raman regimes affects ONR. This transition is illustrated in Fig. 4D as the reversing of the isolation contrast as a function of signal detuning, varying from the Raman regime to the EIT regime and then

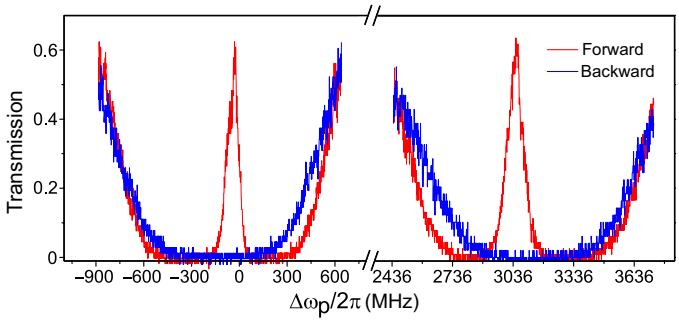

Fig. 5. Double-frequency multiplexed ONR. The nonreciprocal transmission for double-frequency signals with a frequency interval of $2\pi \times 3.036$ GHz.

back to the Raman. The theoretical expectation (solid black curve) agrees well with experimental results. The nonreciprocal contrast takes a positive sign in the EIT regime but becomes negative in the Raman regime. This effect could be applied to control the nonreciprocal directions of the signals by simply tuning the frequency of the control field in the same setup.

Double-frequency multiplexed nonreciprocity

Versatile isolators compatible with a wide range of frequency band or multifrequency channels are attracting considerable attention (*53*, *54*) in optical information processing. As shown in Fig. 5, a double-frequency multiplexed ONR is achieved when the frequency interval of two signals is $\sim 2\pi \times 3.036$ GHz. Essentially, two two-photon transition processes [$5S_{1/2}(F = 3) \rightarrow 5P_{3/2}(F' = 3) \rightarrow 5D_{5/2}(F'' = 4)$ (low-frequency transition) and $5S_{1/2}(F = 2) \rightarrow 5P_{3/2}(F' = 3) \rightarrow 5D_{5/2}(F'' = 4)$ (high-frequency transition)] are exploited to realize ONR in the EIT regime. The forward transmission and isolation for low- and high-frequency signals are {62.4%, 19.1 dB} and {63.5%, 20 dB}, respectively. Overall, we have realized a frequency-multiplexed optical isolation in one channel. This optical isolator can reduce the number of nonreciprocal devices and simplify the configuration for multicolor signals. This achievement also gives a perspective for nonreciprocal devices, working with quantum superposition states encoded in different frequencies.

DISCUSSION

In summary, we have experimentally demonstrated magnetic-free nonreciprocity for single photons (in the EIT regime) and classical fields (in the Raman regime) at room temperature. In the former, the quantum nature of a single photon is maintained (broken) in the forward (backward) direction. The Raman regime enables us to achieve high-performance isolation for a classical field. The demonstrated magnetic-free and reversible optical isolation at room temperature provides a simple building block for reconfigurable quantum networks and integrable optical information processing for hollow-core optical waveguides (*55*) or fibers (*56*) embedded with hot atoms.

MATERIALS AND METHODS

Theoretical simulation

The interaction between photons and atoms in the forward and backward directions is asymmetric, and the interaction Hamiltonian can be written as

$$H_{\text{int}} = -\frac{\hbar}{2}\Big(\Omega_p|2\rangle\langle 1| + \Omega_c|3\rangle\langle 2| - 2\Delta_1|2\rangle\langle 2| - 2(\Delta_1 + \Delta_2)|3\rangle\langle 3|\Big) + h.c. \quad (3)$$

here, $\Omega_p = -\mu_{21}E_p/\hbar$ and $\Omega_c = -\mu_{32}E_c/\hbar$. In addition, μ_{21} (μ_{31}) represents the dipole moment between states $|2\rangle$ ($|3\rangle$) and $|1\rangle$, and E_p (E_c) is the amplitude of the signal photons (control field). Moreover, $\Delta_1 = \Delta\omega_p \pm kv$ is the single-photon detuning when the signal propagates in the forward and backward directions, and $\Delta_2 = \Delta\omega_c - kv$ represents the detuning of the control field, where $\Delta\omega_c$ is set to be $-\Delta\omega_p$ ($-\Delta\omega_p + \delta$) in the EIT (Raman) regime. Then, we can obtain the density matrix element ρ_{21} by solving the steady-state solution of the master equation

$$\frac{\partial\rho}{\partial t} = -\frac{i}{\hbar}[H_{\text{int}}, \rho] - \frac{1}{2}\{\Gamma, \rho\} \quad (4)$$

The second term $\frac{1}{2}\{\Gamma, \rho\}$ on the right-hand side describes the coherence decay of the system. Ultimately, we obtain the respective susceptibility $\chi_{\text{fw(bw)}}$ formula shown in Eqs. 1 and 2. This asymmetric direction-dependent susceptibility in the forward and backward propagation cases induces the nonreciprocity in our scheme. The transmission T_{fw} for the forward and T_{bw} backward propagation cases can be written as

$$T_{\text{fw(bw)}} = \text{Exp}\{-2\text{Im}[(\omega_p/c)(1 + \chi_{\text{fw(bw)}}/2)]L_{\text{eff}}\} \quad (5)$$

where ω_p is the frequency of the photon, c is the speed of light in vacuum, and L_{eff} is the vapor cell effective length.

Generation of a heralded single photon

A pair of nonclassical correlated photons called anti-Stokes and Stokes photons (labeled S1 and S2) are generated through an SFWM process in cold ^{85}Rb atoms. Here, two pump laser beams P1 and P2 are controlled by two acousto-optic modulators modulated by arbitrary function generators (Tektronix, AFG3252) in which the P1 couples the transition $5S_{1/2}(F = 3) \rightarrow 5P_{1/2}(F' = 3)$ with detuning $2\pi \times 70$ MHz, and P2 is resonant with the atomic transition $5S_{1/2}(F = 2) \rightarrow 5P_{3/2}(F' = 3)$. The cold atoms with an optical depth of 10 are trapped in a two-dimensional magneto-optical trap (MOT). The experimental repetition rate is 100 Hz, and the experimental window is 1.3 ms, during which the MOT magnetic field is switched off completely. The P1 and P2 with orthogonal polarization counter-propagate collinearly through the atomic cloud, and hence, their respective signal fields are collinear according to the phase-matching condition, $k_{p1} - k_{S1} = k_{p2} - k_{S2}$, in the SFWM process, as in our previous work (*43*). The photons S1 and S2 are collected at an angle of 3° with respect to the pump lasers, and two lenses with a focal length of 300 mm are used to couple the signal fields into their respective single-mode fibers. The S1 photon is detected by a single-photon detector (avalanche diode, PerkinElmer SPCM-AQR-16-FC; 60% efficiency, maximum dark count rate of 25/s), and the heralded single-photon S2 is prepared for the further demonstration of the single-photon ONR, which is ultimately measured by the single-photon detector. The signals from the two detectors are ultimately sent to a time-correlated single-photon counting system (TimeHarp 260) to measure their time-correlated function.

Characterization of the heralded single-photon

Generally, classical light usually satisfies the Cauchy-Schwarz inequality (*46*) as follows: $R = \left[g^{(2)}_{S1,S2}(\tau)\right]^2 / g^{(2)}_{S1,S1} g^{(2)}_{S2,S2} \leq 1$, where $g^{(2)}_{S1,S2}(\tau)$ is the second-order cross-correlation function, and τ is the relative time delay between signals 1 and 2. Here, $g^{(2)}_{S1,S1}$ and $g^{(2)}_{S2,S2}$ are the autocorrelation functions of signals 1 and 2, respectively. If $R > 1$, the photons are nonclassically correlated, which violates the Cauchy-Schwarz inequality.

The heralded autocorrelation parameter α is usually used to characterize the nature of single-photon sources, which can be written as (*57*) $\alpha = P_1 P_{123} / P_{12} P_{13}$, where P_1 is the count of S1 photons. The S2 photon is separated into two equal parts by a fiber beam splitter, and P_{12} (P_{13}) is the twofold coincidence count between anti-Stokes photon and the corresponding separated Stokes photons. In addition, P_{123} is the threefold coincidence count. For a classical field, $\alpha > 1$. For an ideal single-photon source, $\alpha = 0$, and $\alpha = 0.5$ corresponds to a two-photon state. Therefore, $\alpha < 0.5$ suggests a near-single-photon character.

REFERENCES AND NOTES

1. P. Lodahl, S. Mahmoodian, S. Stobbe, A. Rauschenbeutel, P. Schneeweiss, J. Volz, H. Pichler, P. Zoller, Chiral quantum optics. *Nature* **541**, 473–480 (2017).
2. W. K. Wootters, W. H. Zurek, A single quantum cannot be cloned. *Nature* **299**, 802–803 (1982).
3. J. I. Cirac, P. Zoller, H. J. Kimble, H. Mabuchi, Quantum state transfer and entanglement distribution among distant nodes in a quantum network. *Phys. Rev. Lett.* **78**, 3221 (1997).
4. L. Tang, K. Xia, Optical chirality and single-photon isolation, *Single Photon Manipulation* (IntechOpen, 2019).
5. D. E. Chang, A. S. Sørensen, E. A. Demler, M. D. Lukin, A single-photon transistor using nanoscale surface plasmons. *Nat. Phys.* **3**, 807–812 (2007).
6. J. Lu, L. Zhou, L.-M. Kuang, F. Nori, Single-photon router: Coherent control of multichannel scattering for single photons with quantum interferences. *Phys. Rev. A* **89**, 013805 (2014).
7. B. Hacker, S. Welte, G. Rempe, S. Ritter, A photon-photon quantum gate based on a single atom in an optical resonator. *Nature* **536**, 193–196 (2016).
8. S. Fan, R. Baets, A. Petrov, Z. Yu, J. D. Joannopoulos, W. Freude, A. Melloni, M. Popović, M. Vanwolleghem, D. Jalas, M. Eich, M. Krause, H. Renner, E. Brinkmeyer, C. R. Doerr, Comment on "nonreciprocal light propagation in a silicon photonic circuit". *Science* **335**, 38 (2012).
9. D. Jalas, A. Petrov, M. Eich, W. Freude, S. Fan, Z. Yu, R. Baets, M. Popović, A. Melloni, J. D. Joannopoulos, M. Vanwolleghem, C. R. Doerr, H. Renner, What is – and what is not – an optical isolator. *Nat. Photon.* **7**, 579 (2013).
10. C. Caloz, A. Alù, S. Tretyakov, D. Sounas, K. Achouri, Z. Deck-Léger, Electromagnetic nonreciprocity. *Phys. Rev. Applied* **10**, 047001 (2018).
11. Y. Shi, Z. Yu, S. Fan, Limitations of nonlinear optical isolators due to dynamic reciprocity. *Nat. Photon.* **9**, 388–392 (2015).
12. S. Manipatruni, J. T. Robinson, M. Lipson, Optical nonreciprocity in optomechanical structures. *Phys. Rev. Lett.* **102**, 213903 (2009).
13. Z. Shen, Y.-L. Zhang, Y. Chen, C.-L. Zou, Y.-F. Xiao, X.-B. Zou, F.-W. Sun, G.-C. Guo, C.-H. Dong, Experimental realization of optomechanically induced non-reciprocity. *Nat. Photon.* **10**, 657–661 (2016).
14. E. Verhagen, A. Alù, Optomechanical nonreciprocity. *Nat. Phys.* **13**, 922–924 (2017).
15. Z. R. Gong, H. Ian, Y.-X. Liu, C. P. Sun, F. Nori, Effective Hamiltonian approach to the Kerr nonlinearity in an optomechanical system. *Phys. Rev. A* **80**, 065801 (2009).
16. C.-H. Dong, Z. Shen, C.-L. Zou, Y.-L. Zhang, W. Fu, G.-C. Guo, Brillouin-scattering-induced transparency and non-reciprocal light storage. *Nat. Commun.* **6**, 6193 (2015).
17. B. Peng, Ş. K. Özdemir, F. Lei, F. Monifi, M. Gianfreda, G. L. Long, S. Fan, F. Nori, C. M. Bender, L. Yang, Parity-time-symmetric whispering-gallery microcavities. *Nat. Phys.* **10**, 394–398 (2014).
18. L. Chang, X. Jiang, S. Hua, C. Yang, J. Wen, L. Jiang, G. Li, G. Wang, M. Xiao, Parity-time symmetry and variable optical isolation in active–passive-coupled microresonators. *Nat. Photon.* **8**, 524–529 (2014).
19. I. I. Arkhipov, A. Miranowicz, O. D. Stefano, R. Stassi, S. Savasta, F. Nori, Ş. K. Özdemir, Scully-Lamb quantum laser model for parity-time-symmetric whispering-gallery microcavities: Gain saturation effects and nonreciprocity. *Phys. Rev. A* **99**, 053806 (2019).
20. I. I. Arkhipov, A. Miranowicz, F. Minganti, F. Nori, Quantum and semiclassical exceptional points of a linear system of coupled cavities with losses and gain within the Scully-Lamb laser theory. *Phys. Rev. A* **101**, 013812 (2020).
21. D.-G. Lai, J.-F. Huang, X.-L. Yin, B.-P. Hou, W. Li, D. Vitali, F. Nori, J.-Q. Liao, Nonreciprocal ground-state cooling of multiple mechanical resonators. *Phys. Rev. A* **102**, 011502(R) (2020).
22. H. Xu, L. Jiang, A. A. Clerk, J. G. E. Harris, Nonreciprocal control and cooling of phonon modes in an optomechanical system. *Nature* **568**, 65–69 (2019).
23. J.-H. Wu, M. Artoni, G. C. La Rocca, Non-Hermitian degeneracies and unidirectional reflectionless atomic lattices. *Phys. Rev. Lett.* **113**, 123004 (2014).
24. S. A. R. Horsley, J.-H. Wu, M. Artoni, G. C. La Rocca, Optical nonreciprocity of cold atom Bragg mirrors in motion. *Phys. Rev. Lett.* **110**, 223602 (2013).
25. B. Megyeri, G. Harvie, A. Lampis, J. Goldwin, Directional bistability and nonreciprocal lasing with cold atoms in a ring cavity. *Phys. Rev. Lett.* **121**, 163603 (2018).
26. K. Xia, F. Nori, M. Xiao, Cavity-free optical isolators and circulators using a chiral cross-Kerr nonlinearity. *Phys. Rev. Lett.* **121**, 203602 (2018).
27. M. Scheucher, A. Hilico, E. Will, J. Volz, A. Rauschenbeutel, Quantum optical circulator controlled by a single chirally coupled atom. *Science* **354**, 1577–1580 (2016).
28. C. Sayrin, C. Junge, R. Mitsch, B. Albrecht, D. O'Shea, P. Schneeweiss, J. Volz, A. Rauschenbeutel, Nanophotonic optical isolator controlled by the internal state of cold atoms. *Phys. Rev. X* **5**, 041036 (2015).
29. S. Zhang, Y. Hu, G. Lin, Y. Niu, K. Xia, J. Gong, S. Gong, Thermal-motion-induced non-reciprocal quantum optical system. *Nat. Photon.* **12**, 744–748 (2018).
30. M.-X. Dong, Y.-C. Yu, Y.-H. Ye, W.-H. Zhang, E.-Z. Li, L. Zeng, G.-C. Guo, D.-S. Ding, B.-S. Shi, Experimental realization of quantum non-reciprocity based on cold atomic ensembles. arXiv:1908.09242 (2019).
31. D.-W. Wang, H.-T. Zhou, M.-J. Guo, J.-X. Zhang, J. Evers, S.-Y. Zhu, Optical diode made from a moving photonic crystal. *Phys. Rev. Lett.* **110**, 093901 (2013).
32. K. Xia, G. Lu, G. Lin, Y. Cheng, Y. Niu, S. Gong, J. Twamley, Reversible nonmagnetic single-photon isolation using unbalanced quantum coupling. *Phys. Rev. A* **90**, 043802 (2014).
33. R. Huang, A. Miranowicz, J.-Q. Liao, F. Nori, H. Jing, Nonreciprocal photon blockade. *Phys. Rev. Lett.* **121**, 153601 (2018).
34. A. Miranowicz, J. Bajer, M. Paprzycka, Y.-X. Liu, A. M. Zagoskin, F. Nori, State-dependent photon blockade via quantum-reservoir engineering. *Phys. Rev. A* **90**, 033831 (2014).
35. K.-J. Boller, A. Imamoğlu, S. E. Harris, Observation of electromagnetically induced transparency. *Phys. Rev. Lett.* **66**, 2593–2596 (1991).
36. M. Fleischhauer, A. Imamoglu, J. P. Marangos, Electromagnetically induced transparency: Optics in coherent media. *Rev. Mod. Phys.* **77**, 633–673 (2005).
37. M. Lobino, C. Kupchak, E. Figueroa, A. I. Lvovsky, Memory for light as a quantum process. *Phys. Rev. Lett.* **102**, 203601 (2009).
38. K. Honda, D. Akamatsu, M. Arikawa, Y. Yokoi, K. Akiba, S. Nagatsuka, T. Tanimura, A. Furusawa, M. Kozuma, Storage and retrieval of a squeezed vacuum. *Phys. Rev. Lett.* **100**, 093601 (2008).
39. M. Xiao, Y.-Q. Li, S.-Z. Jin, J. Gea-Banacloche, Measurement of dispersive properties of electromagnetically induced transparency in rubidium atoms. *Phys. Rev. Lett.* **74**, 666–669 (1995).
40. V. Balić, D. A. Braje, P. Kolchin, G. Y. Yin, S. E. Harris, Generation of paired photons with controllable waveforms. *Phys. Rev. Lett.* **94**, 183601 (2005).
41. S. Du, J. Wen, M. H. Rubin, Narrowband biphoton generation near atomic resonance. *JOSA B* **25**, C98–C108 (2008).
42. J. Gea-Banacloche, Y.-q. Li, S.-z. Jin, M. Xiao, Electromagnetically induced transparency in ladder-type inhomogeneously broadened media: Theory and experiment. *Phys. Rev. A* **51**, 576–584 (1995).
43. D.-S. Ding, Z.-Y. Zhou, B.-S. Shi, G.-C. Guo, Single-photon-level quantum image memory based on cold atomic ensembles. *Nat. Commun.* **4**, 2527 (2013).
44. M. D. Reid, D. F. Walls, Violations of classical inequalities in quantum optics. *Phys. Rev. A* **34**, 1260–1276 (1986).
45. G. S. Agarwal, Nonclassical statistics of fields in pair coherent states. *JOSA B* **5**, 1940–1947 (1988).
46. A. Kuzmich, W. P. Bowen, A. D. Boozer, A. Boca, C. W. Chou, L.-M. Duan, H. J. Kimble, Generation of nonclassical photon pairs for scalable quantum communication with atomic ensembles. *Nature* **423**, 731–734 (2003).
47. S. Zhang, J. F. Chen, C. Liu, M. M. T. Loy, G. K. L. Wong, S. Du, Optical precursor of a single photon. *Phys. Rev. Lett.* **106**, 243602 (2011).
48. F. Biraben, The first decades of Doppler-free two-photon spectroscopy. *C. R. Phys.* **20**, 671–681 (2019).
49. D.-S. Ding, W. Zhang, Z.-Y. Zhou, S. Shi, B.-S. Shi, G.-C. Guo, Raman quantum memory of photonic polarized entanglement. *Nat. Photon.* **9**, 332–338 (2015).
50. D.-S. Ding, W. Zhang, Z.-Y. Zhou, S. Shi, G.-Y. Xiang, X.-S. Wang, Y.-K. Jiang, B.-S. Shi, G.-C. Guo, Quantum storage of orbital angular momentum entanglement in an atomic ensemble. *Phys. Rev. Lett.* **114**, 050502 (2015).
51. F. Reiter, A. S. Sørensen, Effective operator formalism for open quantum systems. *Phys. Rev. A* **85**, 032111 (2012).

52. B. Peng, Ş. K. Özdemir, W. Chen, F. Nori, L. Yang, What is and what is not electromagnetically induced transparency in whispering-gallery microcavities. *Nat. Commun.* **5**, 5082 (2014).
53. E. A. Kittlaus, N. T. Otterstrom, P. Kharel, S. Gertler, P. T. Rakich, Non-reciprocal interband Brillouin modulation. *Nat. Photon.* **12**, 613–619 (2018).
54. Y. Hu, S. Zhang, Y. Qi, G. Lin, Y. Niu, S. Gong, Multiwavelength magnetic-free optical isolator by optical pumping in warm atoms. *Phys. Rev. Applied* **12**, 054004 (2019).
55. R. Ritter, N. Gruhler, W. Pernice, H. Kübler, T. Pfau, R. Löw, Atomic vapor spectroscopy in integrated photonic structures. *Appl. Phys. Lett.* **107**, 041101 (2015).
56. V. Venkataraman, K. Saha, A. L. Gaeta, Phase modulation at the few-photon level for weak-nonlinearity-based quantum computing. *Nat. Photon.* **7**, 138–141 (2013).
57. P. Grangier, G. Roger, A. Aspect, Experimental evidence for a photon anticorrelation effect on a beam splitter: A new light on single-photon interferences. *EPL* **1**, 173–179 (1986).

Acknowledgments: We thank C.-H. Dong for discussions. **Funding:** This work was supported by the National Key R&D Program of China (grant nos. 2017YFA0304800, 2019YFA0308700, 2017YFA0303703, and 2019YFA0308704), the National Natural Science Foundation of China (grant nos. 61525504, 61722510, 61435011, 11934013, 11604322, 11874212, 11890704, and U20A20218), the Innovation Fund from CAS, the Anhui Initiative in Quantum Information Technologies (AHY020200), the Fundamental Research Funds for the Central Universities, and the Youth Innovation Promotion Association of CAS under grant no. 2018490. F.N. was supported in part by NTT Research, Army Research Office (ARO) (grant no. W911NF-18-1-0358), the Japan Science and Technology Agency (JST) (via the CREST grant no. JPMJCR1676), the Japan Society for the Promotion of Science (JSPS) (via the KAKENHI grant no. JP20H00134 and the JSPS-RFBR grant no. JPJSBP120194828), the Asian Office of Aerospace Research and Development (AOARD), and the Foundational Questions Institute Fund (FQXi) via grant no. FQXi-IAF19-06. **Author contributions:** M.-X.D. conceived the idea with discussions with D.-S.D. and B.-S.S. M.-X.D carried out the experiments with assistance from D.-S.D., W.-H.Z., and Y.-C.Y. All authors contributed to the discussions and analysis of the results. M.-X.D., K.-Y.X., and D.-S.D. wrote the manuscript with contributions from B.-S.S. and F.N. F.N., K.-Y.X., D.-S.D., B.-S.S., and G.-C.G. supervised the project. **Competing interests:** The authors declare that they have no competing interests. **Data and materials availability:** All data needed to evaluate the conclusions in the paper are present in the paper. Additional data related to this paper may be requested from the authors.

Submitted 21 September 2020
Accepted 26 January 2021
Published 19 March 2021
10.1126/sciadv.abe8924

Citation: M.-X. Dong, K.-Y. Xia, W.-H. Zhang, Y.-C. Yu, Y.-H. Ye, E.-Z. Li, L. Zeng, D.-S. Ding, B.-S. Shi, G.-C. Guo, F. Nori, All-optical reversible single-photon isolation at room temperature. *Sci. Adv.* **7**, eabe8924 (2021).

Science Advances

All-optical reversible single-photon isolation at room temperature

Ming-Xin Dong, Ke-Yu Xia, Wei-Hang Zhang, Yi-Chen Yu, Ying-Hao Ye, En-Ze Li, Lei Zeng, Dong-Sheng Ding, Bao-Sen Shi, Guang-Can Guo and Franco Nori

Sci Adv **7** (12), eabe8924.
DOI: 10.1126/sciadv.abe8924

Science Advances (ISSN 2375-2548) is published by the American Association for the Advancement of Science, 1200 New York Avenue NW, Washington, DC 20005. The title *Science Advances* is a registered trademark of AAAS.